

Towards stable lithium-sulfur batteries: Mechanistic insights into electrolyte decomposition on lithium metal anode



Xiang Chen^{a,1}, Ting-Zheng Hou^{a,1}, Bo Li^b, Chong Yan^{a,c}, Lin Zhu^a, Chao Guan^a, Xin-Bing Cheng^a, Hong-Jie Peng^a, Jia-Qi Huang^{a,d}, Qiang Zhang^{a,*}

^a Beijing Key Laboratory of Green Chemical Reaction Engineering and Technology, Department of Chemical Engineering, Tsinghua University, Beijing 100084, China

^b Shenyang National Laboratory for Materials Science, Institute of Metal Research, Chinese Academy of Sciences, 72 Wenhua Road, Shenyang 110016, China

^c National & Local Joint Engineering Laboratory for Motive Power and Key Materials, College of Chemistry and Chemical Engineering, Henan Normal University, Xinxiang 453007, China

^d Advanced Research Institute for Multidisciplinary Science, Beijing Institute of Technology, Beijing 100081, China

ARTICLE INFO

Keywords:

Lithium-sulfur batteries
Electrolyte
Lithium metal
Carbon
Pouch cell

ABSTRACT

Lithium (Li) metal battery is strongly considered as one of the potential candidates for next-generation energy storage devices due to its ultrahigh energy density. However, gas evolution induced by spontaneous decomposition of organic electrolytes during cell cycling leads to the capacity decay and safety issues of Li metal batteries (LMBs). Herein, the gas evolution behavior in a working Li-sulfur (Li-S) battery based on the most widely used 1,3-dioxolane (DOL)/1,2-dimethoxyethane (DME) electrolyte was probed through gas phase chromatography, mass spectrum of as-produced gas in pouch cells, as well as the first-principles calculations and *ab initio* molecular dynamics. An adsorption-to-reaction mechanism that DOL/DME firstly adsorbed lithium and then decomposed was proposed and verified. DOL with a small decomposition barrier was found to be easily decomposed into ethylene. When the DME:DOL ratio in the organic of Li-S cell was increased, a high and long discharge plateau as well as a large discharge capacity were observed. We also protected Li metal anode to avoid the direct contact between electrolyte and fresh Li metal through the polysulfide additives. The as-obtained cell afforded few gas evolution and consequently a long cycling life. This understanding sheds fresh light of ultra-long cycling life of Li-S pouch cell from the viewpoint of stable electrolyte based on theoretical predictions and experimental verifications, which can be extended to other LMBs based on multi-electron redox reactions.

1. Introduction

Owing to the increasing population and rapid development of modern society, global energy consumption will double from 2010 to 2050 [1]. Consequently, a ravenous demand for high energy storage systems is urgently raised. Among various available anode materials for battery energy storage systems, lithium (Li) metal has the lowest electrode potential (-3.04 V *vs.* standard hydrogen electrode) and an ultrahigh theoretical capacity (3860 mAh g^{-1}) [2,3]. Therefore, Li metal anode have been strongly considered by scientific and engineering community for high-energy-density batteries. When Li metal anode matches sulfur (S) cathode to form a Li-S cell, it can deliver a high theoretical energy capacity of 2600 Wh kg^{-1} , which is 5 times relative to that of conventional Li ion battery (500 Wh kg^{-1}). Li-S battery with

sulfur cathode and lithium anode is highly attractive as the next-generation secondary battery system [4–9].

With the rapid development of material chemistry and energy science, significant progress has been achieved to overcome the intrinsic dilemma of Li-S batteries (*e.g.* poor electrical conductivity of sulfur and its reduced products (Li_2S and Li_2S_2), the dissolution of Li polysulfide intermediates, the instability of electrolytes, and the growth of lithium dendrites). A family of conductive scaffolds, such as porous carbon, carbon nanotubes, graphene, conductive polymer, and various types of hybrids have been employed as 3D interlinked electron pathways of cathode materials [10–13]. To tackle the notorious problem of polysulfide dissolution, the use of heteroatom doping (like B, O, N, P, S, F) [14] and additives (like TiS_2 , ZrS_2 , VS_2 , CoS_2 , Ti_4O_7 , TiO_2 , ZrO_2 , MXene, TiC, VN, NiFe LDH) [15–17] have been proposed

* Corresponding author.

E-mail address: zhang-qiang@mails.tsinghua.edu.cn (Q. Zhang).

¹ These authors contributed equally to this work.

to anchor polysulfide intermediates and promote their redox reactions in a working cell. The introduction of multifunctional electrolyte to regulate polysulfide diffusion and deposition is another effective strategy to retard the polysulfide shuttle for high stable Li-S cells [18–20]. However, when a full Li-S cell is built, the spontaneous reactions between the organic electrolyte and Li metal induce the notorious combustible gas from the decomposition of electrolytes and unstable solid electrolyte interfaces (SEI) on the Li anode [21], which becomes a dominate reason for very short cycling life of Li-S pouch cell with large capacity.

In most cases, the electrolyte should meet some basic criteria (stability, conductivity, solubility of polysulfides, etc.) to serve as interconnected ion channels between cathode and anode in a working cell [22, 23]. Carbonate solvents [24–26], ether solvents [27–33], sulfone homologs [34, 35], aprotic ionic liquids [36], solvate ionic liquids [37, 38], aqueous electrolytes [39, 40], and polymer electrolytes [41] have been explored as electrolytes in Li-S batteries. Among them, 1.0 M lithium bis(trifluoromethanesulfonyl)imide (LiTFSI) in 1,3-dioxane (DOL)/1,2-dimethoxyethane (DME) (1:1 in volume) solution is the most widely used electrolyte in Li-S system for its low viscosity, high polysulfide solubility, good rate capacity, high donor number, and large ionic conductivity [42, 43]. Even though DOL and DME molecules have a relative low reduction potential than most carbonate and ether solvents [44], the gas evolution is still observed in the DOL/DME electrolytes based Li-S batteries, leading to the significant degradation of cell performance. Recently, Hu and co-workers [45] proposed the 'Solvent-in-Salt' electrolyte with high salt concentration and large Li^+ transference number for Li-S cells. The obtained Li-S cells render a coulombic efficiency around 100% and a high cycling stability. Zhang and co-workers [46] adopted another kind of highly concentrated electrolytes (4.0 M lithium bis(fluorosulfonyl)imide (LiTFSI) salt in DME) to achieve more than 6000 cycles at 10 mA cm^{-2} in a lithium metal symmetric cell. Though some progress has been achieved, the mechanism for gas evolution of a Li-S battery is still elusive. There is abundant space to be explored in electrolyte systems to full meet the safe use of Li and S active materials in LMBs.

To avoid the costly trial-and-error test of novel electrolyte, theoretical predictions have been carried out to guide the rational design of organic electrolyte for Li-S batteries. For instance, Park et al. [44] adopted reduction potential as the descriptor to screen organic solvent for lithium metal anode, finding that most ether solvents were relatively stable with a reduction potential lower than -1.40 eV ; Balbuena and co-workers [47–50] pioneered the exploration on the decomposition mechanism of ethylene carbonate [51] at lithium and related surfaces, indicating that the degree of lithiation and nature of exposed surface played a critical role on promoting the decomposition reactions. However, the reason why gas evolution reactions occur in the most used and relatively stable DOL/DME solvents and the corresponding reaction mechanisms are still unclear. This strongly impedes the rational design of effective and safe electrolytes system for high-performance LMBs.

In this contribution, we firstly analyzed the decomposition of organic electrolyte in a pouch cell and determined the composition of exhaust gas in a pouch cell by gas phase chromatography and mass spectrum characterizations. Then, multi-scale calculations, including first-principles calculations and *ab initio* molecular dynamics (AIMD), were performed to focus on gas evolution in DOL/DME solvent based Li-S batteries. An adsorption-to-reaction mechanism was proposed and the reaction process was visually presented. Based on these rigorous theoretical analysis, a feasible battery design strategy was proposed to build stable solid electrolyte interface between lithium anode and electrolytes in a Li-S cell, which promotes discharge capacity from 765 to 840 mAh g^{-1} and coulombic efficiency from 80 to 94% at 100th cycle.

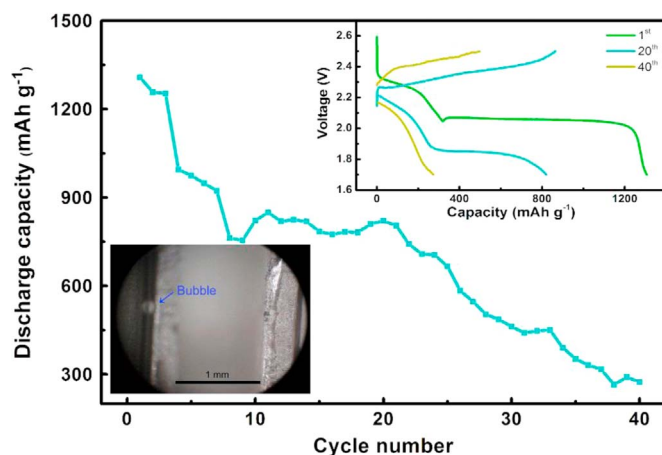


Fig. 1. A long-term cycling test of Li-S pouch cell. The inset figure exhibits the initial, 20th and 40th discharge capacity of the pouch cell. The image is collected from an *in-situ* characterization of the gassing progress in a working Li-cell under optical microscopy.

2. Results and discussion

2.1. Gas evolution in a Li-S pouch cell

Recently, gas evolution was widely observed in Li-S cells during long-term tests [52, 53]. In our test of 40 charge and discharge cycles, the pouch cell was expanded and filled with around 5.1 mL gas (Fig. S1). A gas generation rate is estimated to be $2.09 \times 10^{-8} \text{ mol m}^{-2} \text{ s}^{-1}$ at 300 K (See more details in Supporting text for estimation of gas evolution rate in Supporting Information). The battery capacity decayed from 1308 to 273 mAh g^{-1} , which is faster than a coin cell. Compared to coin cells, the very high areal sulfur loading in pouch cells not only leads to severe shuttle of lithium polysulfides, but also large areal current and high Li plating/stripping of Li anode in a working cell [21, 54]. The reactive solid electrolyte interfaces on Li metal anodes is not very stable and fresh Li metal is easily exposed. The unstable Li metal surface induces the rapid decay of organic electrolyte as well as the formation of Li dendrites under harsh condition. Consequently, the capacity decay of a pouch cell is very rapid. Besides, the gas evolution progress was revealed by *in-situ* characterization under microscopy (in set figure in Fig. 1). Both gas phase chromatography and mass spectrum characterizations were applied to confirm the electrolyte decomposition gas components, showing that ethylene, methane, and ethane were the major gas components. Comparatively, ethylene was confirmed as the main gas product of ethylene carbonate (EC), vinylene carbonate (VC), and tetra(ethylene glycol) dimethyl ether (TEGDME) electrolytes [55–57]. The generated gases are mainly combustible and may cause serious hazards. Therefore, we meet the following questions: 1. How is the intrinsic stability of current DOL/DME electrolyte and what is the key component that promoting their decomposition in a cell? 2. What is the reaction pathway of gas evolution in a working cell? 3. How to minimize the formation of gas formation in an actual cell?

2.2. The intrinsic stability of organic solvent on fresh Li metal

To probe the operation window of different solvents, we firstly check the molecular orbital of DOL, DME (Fig. 2a and b), and EC, which have been widely applied in lithium ion batteries (LIBs). According to the frontier molecular orbital theory, a molecule with a lower lowest unoccupied molecular orbital (LUMO) that is easier to be occupied by electron according to the principle of minimum energy, is very easy to be reduced. In this view, EC molecule, one of the most used solvent in LIBs, has stronger reactivity with lithium metal than DOL/DME (Fig. 3a). Therefore, EC based electrolyte is not suitable for the LMB without Li metal protection strategy. Meanwhile, DOL and DME

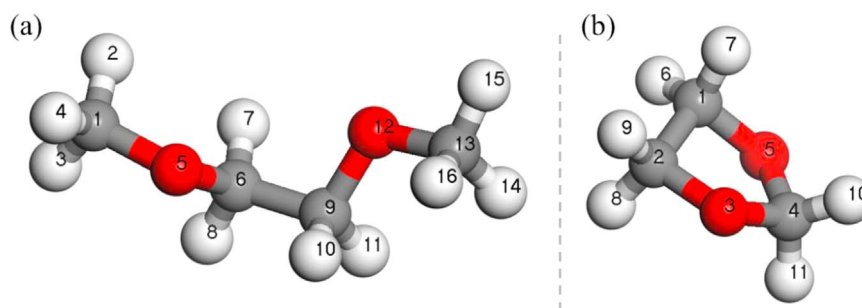


Fig. 2. Atomic number labeling of (a) DME and (b) DOL molecule. The hydrogen, carbon and oxygen atom were marked with white, gray, and red, respectively. (For interpretation of the references to color in this figure legend, the reader is referred to the web version of this article.)

molecules exhibit improved stability with lithium, because the LUMO energy of DOL and DME is a bit higher than the energy level corresponding to Li^+/Li electrode potential (-3.04 V relative to standard hydrogen electrode potential and 1.40 V [58, 59] relative to vacuum in DFT calculation), in accordance with the fact that the DOL/DME based electrolytes are the most widely-used electrolyte in Li-S battery. Nevertheless, DOL/DME electrolyte still decomposes during long-term electrochemical test and gas products are achieved spontaneously (Fig. S1). The decomposition of DOL/DME electrolyte is induced by polarization of electrode, radicals like $\text{S}_3^{\cdot-}$ in electrolyte, ions in electrolyte (like Li^+), trace water, electric field, and so on [52, 60–65].

In order to understand the key component inducing the decomposition of DOL and DME molecules, the LUMO levels of DOL/DME

+X cluster (X=lithium metal, lithium ion, $\text{S}_3^{\cdot-}$ radical, and water) were investigated (Fig. 4 and Table 1). The lithium metal, lithium ions, and $\text{S}_3^{\cdot-}$ radicals significantly reduce the LUMO level of DOL/DME+X cluster (around 2.0 eV , compared with that of DOL/DME). It should be noted that the LUMO of DOL/DME+ $\text{S}_3^{\cdot-}$ cluster is only contributed by S atom, indicating that it is S atom that is firstly reduced rather than DOL or DME molecule. Hence, Li ion is considered as the key component causing the decomposition of DOL and DME molecules, which is consistent with the cognition at experimental level.

2.3. Reaction pathway of electrolyte decomposition

From the analysis of frontier molecular orbital, Li ion was confirmed as key component causing the decomposition of DOL and

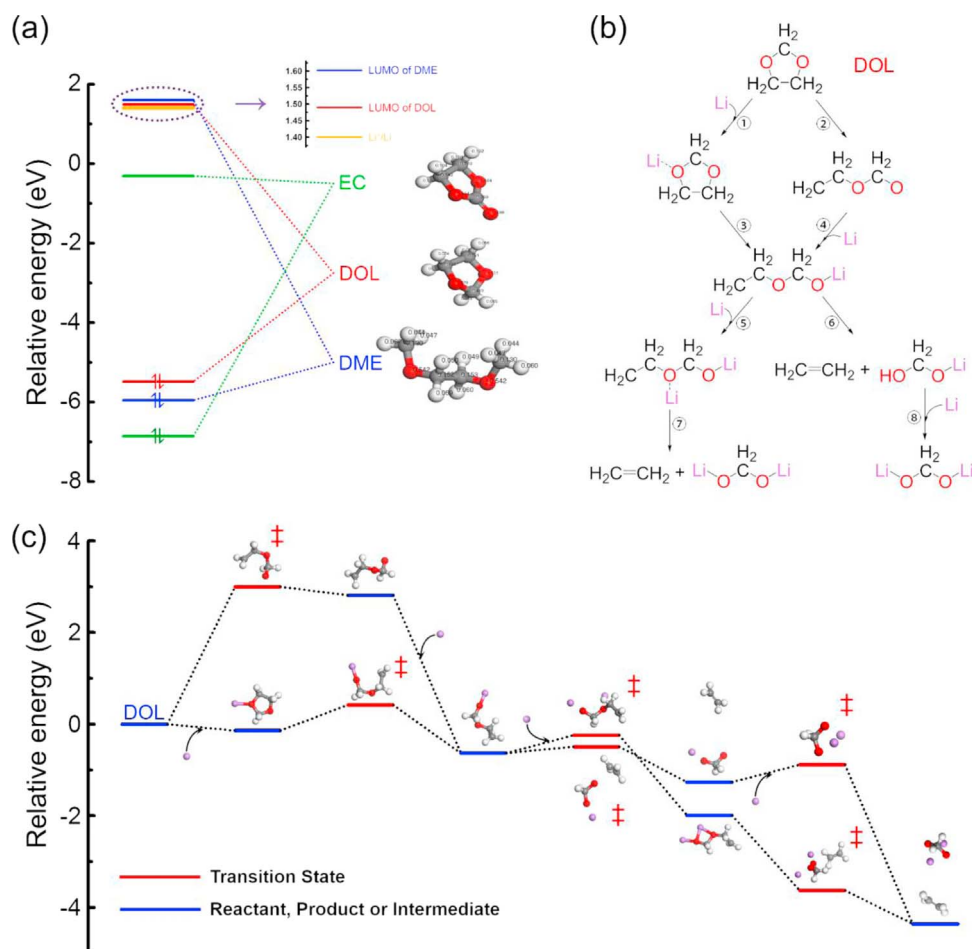


Fig. 3. (a) HOMO and LUMO energy comparison of EC, DOL, and DME molecules. Mulliken charge is also presented near atoms. (b) Reaction net of DOL decomposition mechanism. (c) Decomposition reaction pathway of DOL molecule. The hydrogen, lithium, carbon, and oxygen atom were marked with white, purple, gray, and red, respectively. (For interpretation of the references to color in this figure legend, the reader is referred to the web version of this article.)

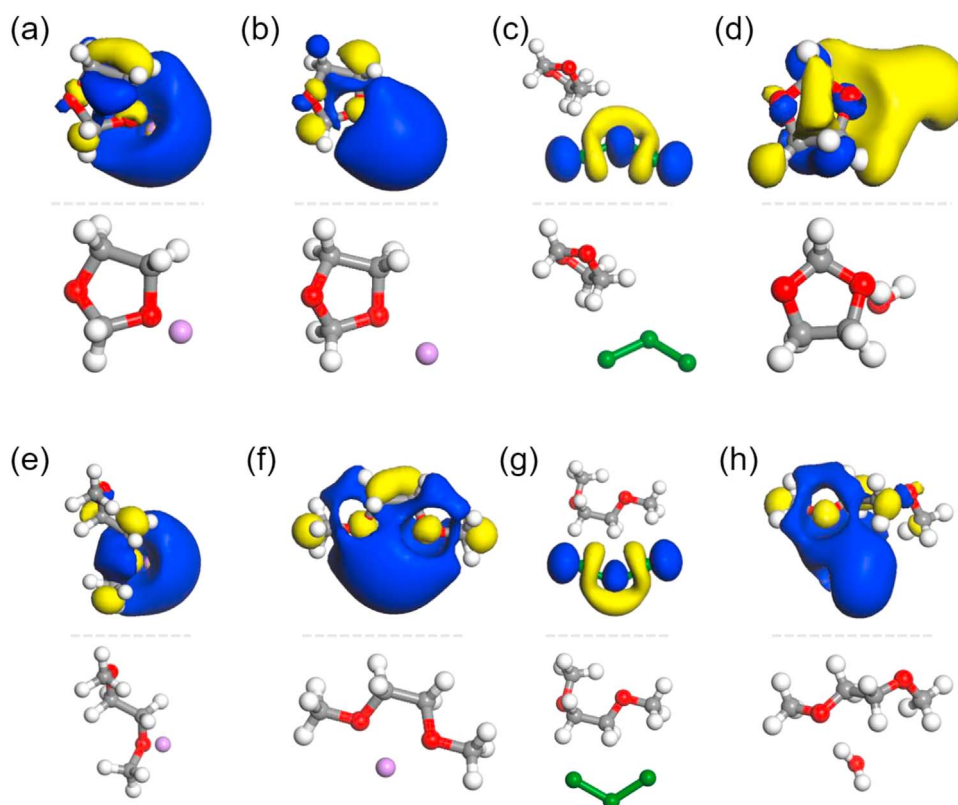


Fig. 4. Visual LUMO and corresponding geometry structure of (a) DOL+Li; (b) DOL+Li⁺; (c) DOL+S₃⁻; (d) DOL+H₂O; (e) DME+Li; (f) DME+Li⁺; (g) DME+S₃⁻; (h) DME+H₂O. The hydrogen, lithium, carbon, oxygen, and sulfur atom were marked with white, purple, gray, red, and green, respectively. The blue and yellow region represent the positive and negative parts of the LUMO wave function, respectively. (For interpretation of the references to color in this figure legend, the reader is referred to the web version of this article.)

Table 1

Reduced Energy of LUMO of DME and DOL molecule interacting with lithium atom, lithium ion, S₃⁻ radical and water molecule, considering solvation.

Reduced Energy of LUMO	DOL (eV)	DME (eV)
Li atom	-1.98	-2.21
Li ⁺ ion	-2.24	-2.26
S ₃ ⁻	-1.64	-1.75
H ₂ O	-0.41	-0.28

DME. The adsorbed lithium preferred to bind with oxygen atom in DOL and DME molecules, indicating a possible reactive site. In order to identify possible reaction routes between lithium and DOL/DME solvent, overlap population analysis (a bond with little overlap population is easy to be broken) [66, 67] was applied to determine the weakest bond in DOL and DME molecules. As shown in Table S1, C1-O5 and C1-O5/C13-O12 are the weakest bond in DOL and DME, respectively. Moreover, C6-O5/C9-O12 bond in DME was easier to be broken than C1-O5/C13-O12, showing differences with overlap population analysis. A comprehensive reaction net, including 22 reactions between lithium and DOL/DME molecule, was then proposed in Fig. 3b and S2.

According to the priority of adsorption and reaction, the reaction pathways are classified as adsorption-to-reaction and reaction-to-adsorption route. For instance, in the adsorption-to-reaction route (Reaction 1→Reaction 3), lithium was adsorbed on oxygen atom in DOL firstly and then DOL opened the ring; in the reaction-to-adsorption route (Reaction 2→Reaction 4), DOL opened the ring firstly and then lithium was adsorbed on the oxygen atom in intermediate compound. Notably, methane, ethane, and ethylene are the final gas products in Reaction 6, 7, 13, 15, 21, and 22. In addition, most of 22 reactions are exothermic except Reaction 2, 6, 10, 11, 13, and 18, indicating the feasibility from the viewpoint of thermodynamics (Table

S2). Considering the ring opening reaction of DOL, the reaction energy change is exothermic by -0.27 eV and endothermic by 3.13 eV in Reaction 3 and 2, respectively. The only difference between Reaction 2 and 3 was whether lithium takes part in the ring opening process or not. The result manifests the important role of lithium in promoting the decomposition of DOL molecule. Similar regularity can be concluded from comparing Reaction 10 and 11, Reaction 13 and 15, Reaction 18 and 19. This was in consistency with the decomposition of EC that ring-open reaction of lithium-ion-coordinated molecules were exothermic and isolated solvent molecules were endothermic [61, 68].

To probe the kinetic of DOL/DME decomposition based on above proposed reaction pathway, transition state search was performed (Fig. 3c and S3). The most favorable reaction path of DOL decomposition (Fig. 3b) was Reaction 1→Reaction 3→Reaction 5→Reaction 7, exhibiting an adsorption-to-reaction mechanism. The rate determining step was Reaction 3 (ring opening reaction) with a maximum energy barrier of 0.56 eV. Comparatively, Bedrov [69] predicted the ring-opening reaction of EC with a barrier of 0.48–0.52 eV under ReaxFF simulations. The whole process of decomposition is divided into two stage according to the number of lithium participating in the reaction like the two-electron reduction processes of EC [70]: stage 1 (Reaction 1 and Reaction 3) and stage 2 (Reaction 5 and Reaction 7). The second stage reaction has a very small reaction barrier of 0.34 eV. Once the DOL ring was open under the interaction of first lithium, the subsequent reactions proceed rapidly. When comparing the two different mechanisms of ring opening reactions, adsorption-to-reaction mechanism with a barrier of 0.56 eV was much more favorable than reaction-to-adsorption mechanism with a barrier of 3.00 eV, which highlighted the critical role of lithium in promoting the decomposition of DOL molecule. The decomposition of DOL molecule by interacting with lithium, was similar to a S_N2 reaction. The oxygen atom (*i.e.* O3) was firstly bound with a lithium ion, and became positively charged. As C2 atom was also positively charged, the C2-O3 bond length increased

from 0.14 to 0.15 nm and became weaker, easier to be broken. Therefore, lithium promoted the broken of carbon-oxygen bond. Similarly, Endo et al. [61, 68] reported that the initial decomposition reaction of EC solvent in LIBs was an electron transfer from the anode to the lithium-ion coordinated solvents, favoring our conclusions.

The decomposition of DME molecule was much more complex as two kinds of carbon-oxygen bonds were broken when interacting with lithium. The reaction path of bond breaking patterns are illustrated in Fig. S2. Similarly, the decomposition of DME preferred an adsorption-to-reaction mechanism. On one hand, the first bond breaking of carbon-oxygen when reacting with lithium (Reaction 11 and 19) was rate determining step of whole decomposition reactions. This underlined the critical role of lithium in promoting the decomposition of DME molecule. On the other hand, the adsorption-to-reaction and reaction-to-adsorption bond breaking patterns rendered approximate reaction barriers of 0.86 and 0.79 eV, respectively (Fig. S3a and S3b). This indicates that DME molecule decomposed in two kinds of mechanisms, differing from DOL molecule. Remarkably, the reaction barrier of DME was larger than that of DOL (0.56 eV) no matter which mechanism prevailed, rendering an improved stability of DME molecule when interacting with lithium anode.

2.4. Gas evolution predicted by the *ab initio* molecular dynamics

To probe the scenario of electrolyte decomposition, an *ab initio* molecular dynamics calculation was carried out based on six slab or cluster models. As summarized in Fig. 5 and Table 2, the lithium atoms that adequately exposed to solvent molecule in a cluster model were

Table 2
Summary of AIMD.

Model	DME	DOL	DME-D	DOL-D
Li (110)+6DME	6	0	0	0
Li-35+14DME	14	0	6	0
Li (110)+9DOL	0	9	0	2
Li-35+20DOL	0	20	0	6
Li (110)+3DME+5DOL	3	5	0	2
Li-35+7DME+10DOL	7	10	2	5

Note: DME-D and DOL-D means the number of decomposed DME/DOL molecule during the 5 ps AIMD.

more active than that in slab models; DME was of better stability than DOL. Specifically, there was no reaction observed between lithium slab and DME molecule during the 5 ps *ab initio* molecular dynamics, while 2 out of 9 DOL molecules decomposed, indicating better stability of DME molecules. Meanwhile, 6 out of 14 DME molecules decomposed when interacting with Li cluster during the 5 ps simulation, demonstrating better reactivity of lithium cluster. This was well consistent with the results in transition state search and favored the proposed adsorption-to-reaction mechanism. In addition, the spontaneous reactions between mixture solvent and lithium are more complex.

The Li (110)+9DOL model was hereby discussed as a typical example. At 1866 fs, a carbon-oxygen bond of a DOL molecule was broken with the interaction of a lithium atom. The distance between the interacting oxygen and lithium atom was 0.19 nm, which was similar to the O-Li distance of 0.20 nm in lithium oxide crystal. A second carbon-oxygen bond in that molecule was broken only 73 fs

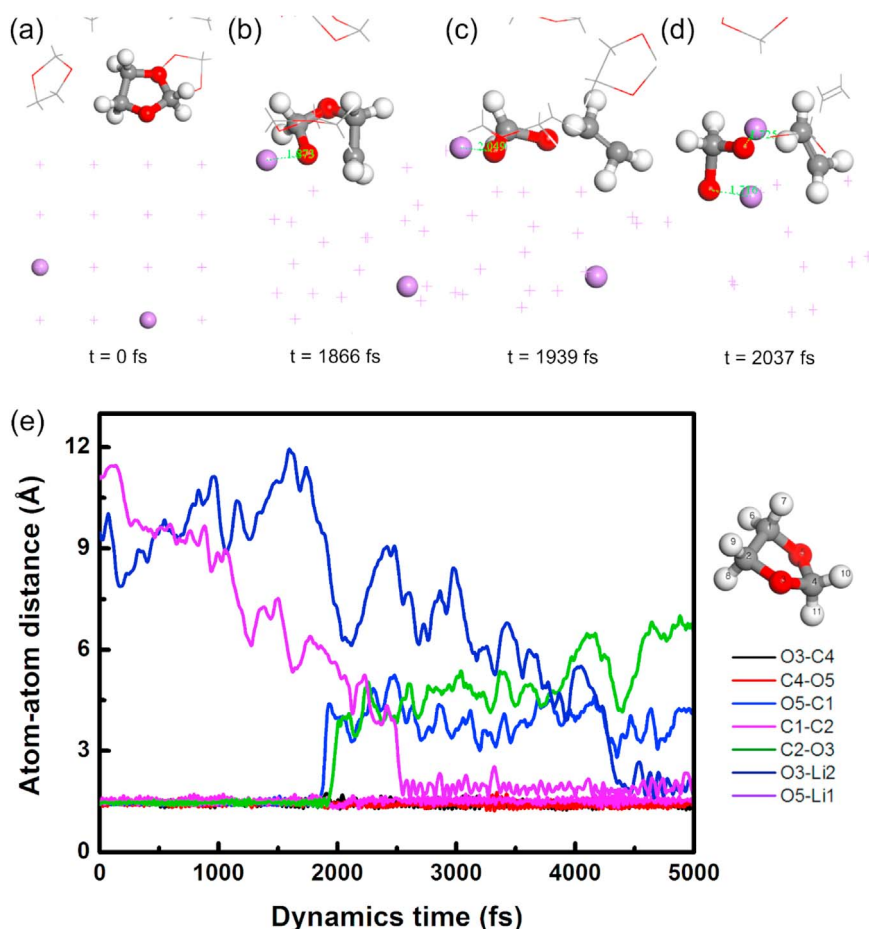


Fig. 5. (a–d) Complete sequence of DOL molecule decomposition obtained from AIMD simulation for Li (110)+9DOL model. (e) Time evolution of another DOL molecule decomposition in the Li (110)+9DOL model. The hydrogen, lithium, carbon, and oxygen atom were marked with white, purple, gray, and red, respectively. (For interpretation of the references to color in this figure legend, the reader is referred to the web version of this article.)

later since the second-stage reaction was much faster than the first-stage reaction, explained in the section of transition state search. It should be articulated that the second carbon-oxygen bond broke when interacting with another lithium atom, which was not shown in this simulation box. The final products, which included an ethylene molecule specifically, formed at 2037 fs and then the ethylene molecule diffused to the liquid phase. Additionally, the time evolution of another decomposed DOL molecule in the Li (110)+9 DOL model is illustrated in Fig. 5e, presenting the atom-atom distance change process during the whole simulation process. At around 1900 fs, two carbon-oxygen bonds were broken one after another, with just a small time gap, indicating that the first-stage reaction is the rate determining step. What should be clarified is that the interacting lithium atom that led to the breaking of carbon-oxygen bond was different from the final adsorptive lithium atom in final products since $\text{CH}_2(\text{Li})_2$ can dissociate and re-adsorb. A more distinct dissociation-to-adsorption process was the distance change of O5-Li1 (dissociated around 3600 fs and re-adsorbed around 4900 fs) as time shown in Fig. S4. More details of AIMD results of other models can be found in Fig. S4–9.

The AIMD results not only presented the main decomposition reactions between DOL/DME solvent and lithium anode, but also explained the formation mechanism of methane and ethane in a real operating condition. The formation of methyl radical was observed during the simulation in Li-35+7DME+10DOL model (Fig. S5) and the formation mechanism was the second decomposition mechanism of DME with a reaction barrier of 0.79 eV (Fig. S3b). Surprisingly, the methyl radicals were relatively stable in this system and kept to the end of simulation. The methyl radicals were more produced in a working cell and their relative stability afforded the possibility of collisions between two methyl radicals, leading to the formation of ethane. What is more, hydrogen was also observed during the simulation in Li-35+14DME model and preferred to bond with lithium. The formation of methyl and hydrogen radicals made it possible to form of methane. Consequently, the AIMD results also provided a deep understanding of gas evolution in Li-S battery.

Besides, a theoretical gas generation rate estimation was performed based on Li (110)+3DME+5DOL model, which was the closest to the actual battery system. There was one ethylene generated during the 5 ps simulation and the theoretical gas generation rate was estimated to be $3.75 \times 10^{-5} \text{ mol m}^{-2} \text{ s}^{-1}$ at 300 K, which was 1796 times larger than the experimental rates (See more details in Supporting Text for estimation of gas evolution rate in Supporting Information). Such difference is attributed from the fact that the actual gas evolution was only clearly observed at the initial period of cycling as decomposed organic or inorganic products piled up on lithium surface and impeded further reactions. Therefore, the overall reaction rate was much lower than the initial gas generation rate (theoretically estimated rate).

2.5. The gas evolution in Li-S cell with different DOL/DME ratio

From the above discussions, DOL is easier to decompose than DME. To reveal the general rule of gas evolution in a Li-S cell with DOL and DME electrolyte, the composition of gas produced in electrolytes with different DOL/DME ratios were probed and listed in Table 3. The proportion of methane in gas increased with the proportion of DME in electrolyte, which agreed well with the above conclusion that methane was

Table 3
Component analysis of the gas produced in Li-S cell.

Components	DOL:DME=1:2	DOL:DME=2:1
CH_4	15%	8%
C_2H_4	81%	85%
C_2H_6	3%	4%
C_3^+	1%	3%

only produced by DME. Furthermore, as indicated by above theoretical predictions from transition state search and AIMD, DME was more stable than DOL. As a result, electrolyte with higher proportion of DME is more stable. The suppressed gas evolution during the charge and discharge process can be anticipated. Based on the above mentioned analysis, Li-S batteries with organic electrolytes with higher DME ratio are expected to render excellent stability. Such simple but efficient concept was verified by experimental tests (Fig. 6a and b). Pouch cell, whose electrolyte consisted with a higher ratio of DME (DOL:DME=1:5), exhibited a higher and longer discharge plateau. This resulted in a much higher discharge capacity (947 mAh g^{-1}) at 27th cycle than that of lower ratio of DME (DOL:DME=2:1, 733 mAh g^{-1}).

2.6. Rational design of stable interface to retard gas evolution

If a very stable interface can be built between electrolyte and reactive lithium metal surface, the as-obtained Li metal cell is without direct contact between electrolyte and the reactive lithium metal [15]. Electroplating a protective SEI film in a polysulfide based electrolyte on the surface of lithium anode [71–73] is expected to separate the electrolyte from active fresh lithium and achieve great long-term performance. To demonstrate this proof of the concept, we proposed a Li-S battery with polysulfides as additive in the organic electrolyte to build stable SEI on Li metal anode (Fig. 7).

The coulombic efficiency of the battery whose anode was electroplated with a mixture of Li_2S_5 and LiNO_3 solution was above 94% in the first 100 cycles, indicating the formation of stable protecting layer on Li metal anode and the reduced reactivity between lithium anode and electrolyte (Fig. 6c). In contrast, the coulombic efficiency of the Li-S battery without anode protection doped to 80% in the 100th-cycle mainly due to the unstable interface between Li anode and electrolytes. Apart from that, the Li-S cell with anode protection can maintain 98.5% of the initial discharge capacity (852 mAh g^{-1}) after 100 cycles; the Li-S battery without anode protection rendered similar initial discharge capacity, but a low capacity of 765 mAh g^{-1} at 100th cycle. This confirmed the feasibility of our proposed strategy that separated reactive lithium from electrolyte to achieve superb long-term performance and verified that the origin of gas evolution in a Li-S battery is the intrinsic reaction between active lithium anode and electrolyte components, sufficiently confirming the calculation results.

2.7. Inspiration for rational design of lithium metal batteries

LMBs have been considered as the Holy Grail batteries. Unfortunately, the growth of lithium dendrites and strong reactivity between lithium anode and electrolytes have impeded its practical implications. The emerging concept to deposit Li onto nanostructured anode were highly explored [74–76]. The controllable regulation of stable interfaces between lithium anode and electrolyte [77–80] is a key issue to guarantee the high utilization of Li metal and afford dendrite-free growth of Li metal. The complex reaction between polysulfides and Li metal have a critical role on the formation of stable solid electrolyte interphase [81, 82]. The intermediated buffer layer (i.e. solid electrolyte) [83–87] not only needs to be strong enough to resist the growth of lithium dendrites and protect electrolyte from continuous decomposition, but also requires extraordinary lithium ionic conductivity and electronic insulation. Furthermore, the buffer layer is expected to be even part of the electrolyte, which is the ultimate goal of battery development, even though the surface interactions between lithium anode and solid electrolyte are still far from clear.

Theoretical simulations afford a deep understanding of interfacial interactions among lithium anode, buffer layer, and electrolytes. The results reported herein confirmed the highly reactive lithium as the key component to promote the decomposition of solvents in Li-S cell and deepen the understanding of the interaction between lithium anode and electrolytes. Up to now, reduction potential, ionization potential,

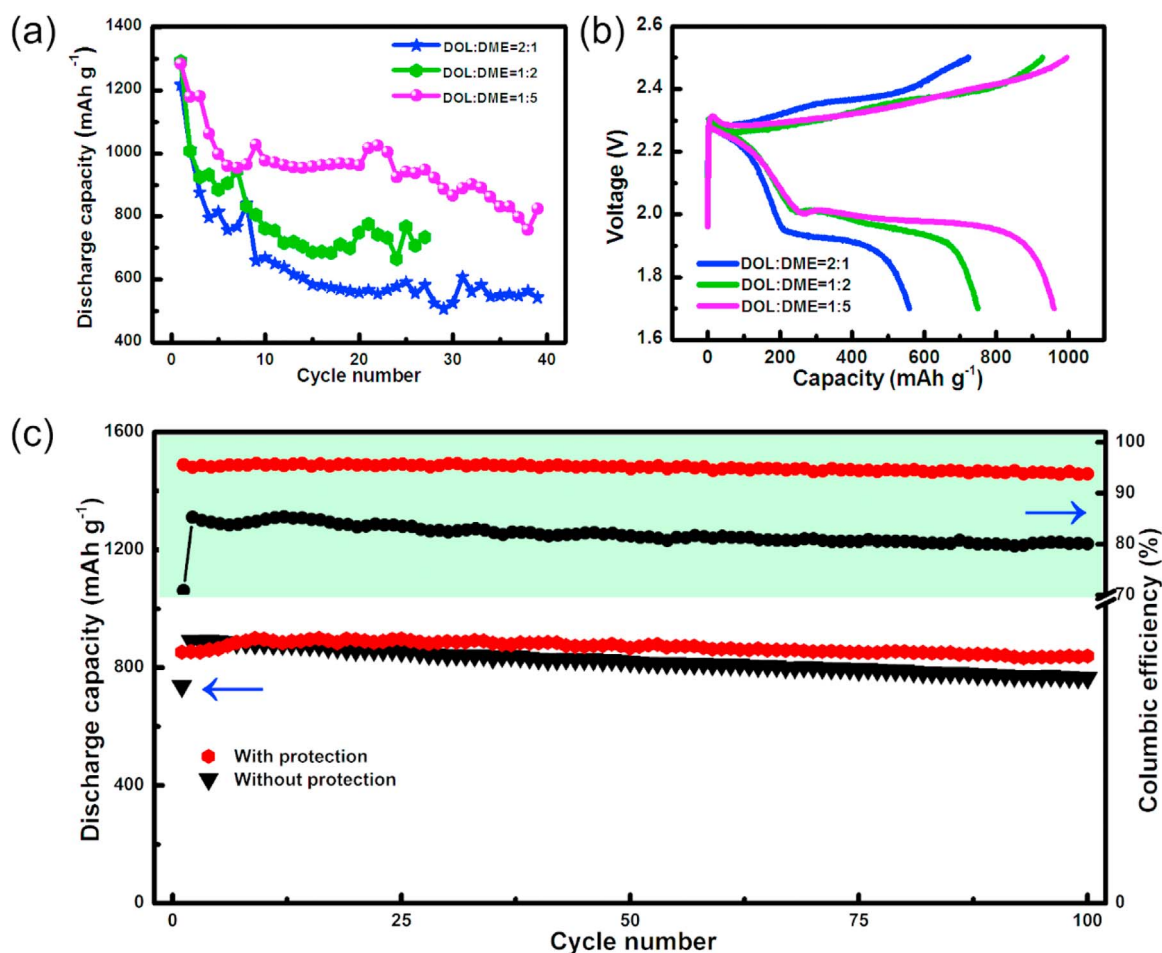


Fig. 6. (a) Long-term cycling test and (b) first-cycle charge and discharge curve of pouch cells with electrolytes of different DOL/DME mass ratio. (c) Long-term cycling test of with and without Li metal protection.

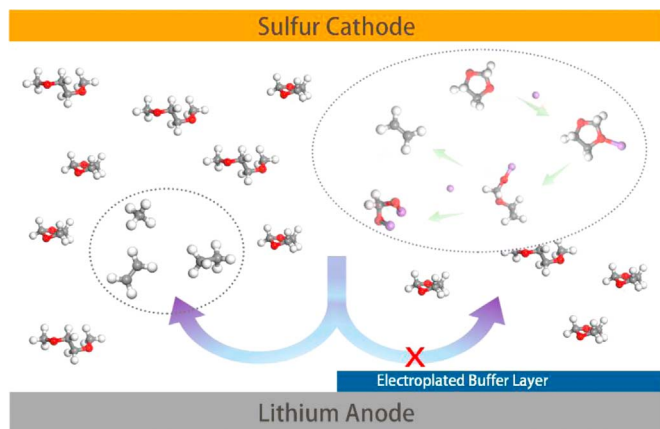


Fig. 7. Rational design of stable interface to regard gas evolution. The gases and the decomposition mechanism of DOL are shown in the two dotted ellipses, respectively.

electron affinities, isothermal diffusion coefficients, and isothermal ionic conductivities have been applied as descriptors to screen electrolytes at theoretical level [44, 88, 89]. Unfortunately, the connection between the calculated descriptors and actual cell performances is still far from clear, resisting a high throughput screening for advanced electrolytes and building the electrolytes materials genome for LMBs. A combined research, connecting the calculated descriptors and experimental performances with chemical/physical/mathematical models, is still requested to realize the screening in real instead of costly trial-and-error tests in electrolyte design.

3. Conclusions

The gas evolution mechanism in Li-S battery based on DOL/DME electrolyte is probed through gas phase chromatography, mass spectrum of as-produced gas in pouch cells, as well as the first-principles calculations and *ab initio* molecular dynamics. The DOL prefers to react with Li metal, while a good stability of DME molecule was confirmed by both theoretical predictions and experimental observations. An adsorption-to-reaction mechanism was proposed based on the multi-scale calculations, illustrating the decomposition mechanism of DOL/DME solvent in Li-S system. Moreover, lithium was confirmed as the key component that leads to gas evolution. Based on this idea, electroplating a protective film on the reactive lithium anode was proposed to separate solvent molecule from reactive Li surface and protect Li anode in a working cell. This work provides a creative and vital understanding to gas evolution in a working Li-S battery and a general principle to design new LMB systems and other batteries with metal anodes.

Acknowledgements

This work was supported by funding from National Key Research and Development Program (No. Key 2016YFA0202500), Natural Scientific Foundation of China (Nos. 21422604, 21676160, and 21561130151), Tsinghua University Initiative Scientific Research Program (No. 20161080166), and Tsinghua National Laboratory for Information Science and Technology. We thank Rui Zhang, Chen-Zi Zhao, Cheng Tang, Wen-Tao Xu, Peng Li, Lida Zhao, and Yingying Zhang at Tsinghua University for helpful discussion.

Appendix A. Supplementary material

Supplementary data associated with this article can be found in the online version at <http://dx.doi.org/10.1016/j.ensm.2017.01.003>.

References

- [1] D. Larcher, J.M. Tarascon, *Nat. Chem.* 7 (2015) 19–29.
- [2] W. Xu, J.L. Wang, F. Ding, X.L. Chen, E. Nasybutin, Y.H. Zhang, J.G. Zhang, *Energy Environ. Sci.* 7 (2014) 513–537.
- [3] X.-B. Cheng, R. Zhang, C.-Z. Zhao, F. Wei, J.-G. Zhang, Q. Zhang, *Adv. Sci.* 3 (2016) 1500213.
- [4] R.G. Cao, W. Xu, D.P. Lv, J. Xiao, J.G. Zhang, *Adv. Energy Mater.* 5 (2015) 1402273.
- [5] A. Manthiram, S.-H. Chung, C. Zu, *Adv. Mater.* 27 (2015) 1980–2006.
- [6] Z.W. Seh, Y. Sun, Q. Zhang, Y. Cui, *Chem. Soc. Rev.* 45 (2016) 5605–5634.
- [7] S.S. Zhang, *J. Power Sources* 231 (2013) 153–162.
- [8] L. Borchardt, M. Oschatz, S. Kaskel, *Chem. Eur. J.* 22 (2016) 7324–7351.
- [9] X. Zhang, X. Cheng, Q. Zhang, *J. Energy Chem.* 25 (2016) 967–984.
- [10] X. Ji, K.T. Lee, L.F. Nazar, *Nat. Mater.* 8 (2009) 500–506.
- [11] M. Yu, R. Li, M. Wu, G. Shi, *Energy Storage Mater.* 1 (2015) 51–73.
- [12] J. Liang, Z.-H. Sun, F. Li, H.-M. Cheng, *Energy Storage Mater.* 2 (2016) 76–106.
- [13] C. Tang, B.Q. Li, Q. Zhang, L. Zhu, H.F. Wang, J.L. Shi, F. Wei, *Adv. Funct. Mater.* 26 (2016) 577–585.
- [14] T.Z. Hou, X. Chen, H.J. Peng, J.Q. Huang, B.Q. Li, Q. Zhang, B. Li, *Small* 12 (2016) 3283–3291.
- [15] Z. Yuan, H.J. Peng, T.Z. Hou, J.Q. Huang, C.M. Chen, D.W. Wang, X.B. Cheng, F. Wei, Q. Zhang, *Nano Lett.* 16 (2016) 519–527.
- [16] X. Tao, J. Wang, C. Liu, H. Wang, H. Yao, G. Zheng, Z.W. Seh, Q. Cai, W. Li, G. Zhou, C. Zu, Y. Cui, *Nat. Commun.* 7 (2016) 11203.
- [17] Q. Pang, X. Liang, C.Y. Kwok, L.F. Nazar, *J. Electrochem. Soc.* 162 (2015) A2567–A2576.
- [18] J.-Q. Huang, Q. Zhang, F. Wei, *Energy Storage Mater.* 1 (2015) 127–145.
- [19] C.H. Chang, S.H. Chung, A. Manthiram, *Small* 12 (2016) 174–179.
- [20] H.J. Peng, D.W. Wang, J.Q. Huang, X.B. Cheng, Z. Yuan, F. Wei, Q. Zhang, *Adv. Sci.* 3 (2016) 1500268.
- [21] X.-B. Cheng, C. Yan, J.-Q. Huang, P. Li, L. Zhu, L. Zhao, Y. Zhang, W. Zhu, S.-T. Yang, Q. Zhang, *Energy Storage Mater.* 6 (2017) 18–25.
- [22] M. Barghamadi, A.S. Best, A.I. Bhatt, A.F. Hollenkamp, M. Musameh, R.J. Rees, T. Ruther, *Energy Environ. Sci.* 7 (2014) 3902–3920.
- [23] L.M. Suo, O. Borodin, T. Gao, M. Olguin, J. Ho, X.L. Fan, C. Luo, C.S. Wang, K. Xu, *Science* 350 (2015) 938–943.
- [24] S. Xin, L. Gu, N.-H. Zhao, Y.-X. Yin, L.-J. Zhou, Y.-G. Guo, L.-J. Wan, *J. Am. Chem. Soc.* 134 (2012) 18510–18513.
- [25] B. Zhang, X. Qin, G.R. Li, X.P. Gao, *Energy Environ. Sci.* 3 (2010) 1531–1537.
- [26] Z. Xu, J. Wang, J. Yang, X. Miao, R. Chen, J. Qian, R. Miao, *Angew. Chem. Int. Ed.* 55 (2016) 10372–10375.
- [27] W. Weng, V.G. Pol, K. Amine, *Adv. Mater.* 25 (2013) 1608–1615.
- [28] S. Kim, Y. Jung, H.S. Lim, *Electrochim. Acta* 50 (2004) 889–892.
- [29] J.-W. Choi, J.-K. Kim, G. Cheruvally, J.-H. Ahn, H.-J. Ahn, K.-W. Kim, *Electrochim. Acta* 52 (2007) 2075–2082.
- [30] C. Barchasz, J.-C. Leprêtre, S. Patoux, F. Alloin, *J. Electrochem. Soc.* 160 (2013) A430–A436.
- [31] S.S. Zhang, *J. Power Sources* 322 (2016) 99–105.
- [32] H. Kim, F.X. Wu, J.T. Lee, N. Nitta, H.T. Lin, M. Oschatz, W.I. Cho, S. Kaskel, O. Borodin, G. Yushin, *Adv. Energy Mater.* 5 (2015) 1401792.
- [33] M. Zhang, C. Yu, C. Zhao, X. Song, X. Han, S. Liu, C. Hao, J. Qiu, *Energy Storage Mater.* 5 (2016) 223–229.
- [34] R. Demir-Cakan, *J. Power Sources* 282 (2015) 437–443.
- [35] S.R. Chen, F. Dai, M.L. Gordin, Z.X. Yu, Y. Gao, J.X. Song, D.H. Wang, *Angew. Chem. Int. Ed.* 55 (2016) 4231–4235.
- [36] L.X. Yuan, J. Feng, X.P. Ai, Y.L. Cao, S.L. Chen, H.X. Yang, *Electrochem. Commun.* 8 (2006) 610–614.
- [37] N. Tachikawa, K. Yamauchi, E. Takashima, J.-W. Park, K. Dokko, M. Watanabe, *Chem. Commun.* 47 (2011) 8157–8159.
- [38] L.N. Wang, J.Y. Liu, S.Y. Yuan, Y.G. Wang, Y.Y. Xia, *Energy Environ. Sci.* 9 (2016) 224–231.
- [39] N. Li, Z. Weng, Y. Wang, F. Li, H.-M. Cheng, H. Zhou, *Energy Environ. Sci.* 7 (2014) 3307–3312.
- [40] J. Shao, X. Li, L. Zhang, Q. Qu, H. Zheng, *Nanoscale* 5 (2013) 1460–1464.
- [41] J. Hassoun, B. Scrosati, *Adv. Mater.* 22 (2010) 5198–5201.
- [42] S. Zhang, K. Ueno, K. Dokko, M. Watanabe, *Adv. Energy Mater.* 5 (2015) 1500117.
- [43] X.B. Cheng, H.J. Peng, J.Q. Huang, R. Zhang, C.Z. Zhao, Q. Zhang, *ACS Nano* 9 (2015) 6373–6382.
- [44] M.S. Park, S.B. Ma, D.J. Lee, D. Im, S.-G. Doo, O. Yamamoto, *Sci. Rep.* 4 (2014) 3815.
- [45] L.M. Suo, Y.S. Hu, H. Li, M. Armand, L.Q. Chen, *Nat. Commun.* 4 (2013) 1481.
- [46] J. Qian, W.A. Henderson, W. Xu, P. Bhattacharya, M. Engelhard, O. Borodin, J.-G. Zhang, *Nat. Commun.* 6 (2015) 6362.
- [47] T. Li, P.B. Balbuena, *Chem. Phys. Lett.* 317 (2000) 421–429.
- [48] J.M. Martínez, de la Hoz, K. Leung, P.B. Balbuena, *ACS Appl. Mater. Interfaces* 5 (2013), 2013, pp. 13457–13465.
- [49] L.E. Camacho-Forero, T.W. Smith, S. Bertolini, P.B. Balbuena, *J. Phys. Chem. C* 119 (2015) 26828–26839.
- [50] K. Leung, F. Soto, K. Hankins, P.B. Balbuena, K.L. Harrison, *J. Phys. Chem. C* 120 (2016) 6302–6313.
- [51] A.D. Becke, *J. Chem. Phys.* 98 (1993) 5648–5652.
- [52] A. Jozwiuk, B.B. Berkes, T. Weiß, H. Sommer, J. Janek, T. Brezesinski, *Energy Environ. Sci.* 9 (2016) 2603–2608.
- [53] B. Michalak, H. Sommer, D. Mannes, A. Kaestner, T. Brezesinski, J. Janek, *Sci. Rep.* 5 (2015) 15627.
- [54] L. Gireaud, S. Grugeon, S. Laruelle, B. Yrieix, J.M. Tarascon, *Electrochem. Commun.* 8 (2006) 1639–1649.
- [55] J.-S. Bridel, S. Grugeon, S. Laruelle, J. Hassoun, P. Reale, B. Scrosati, J.-M. Tarascon, *J. Power Sources* 195 (2010) 2036–2043.
- [56] M.M. Islam, V.S. Bryantsev, A.C.T. van Duin, *J. Electrochem. Soc.* 161 (2014) E3009–E3014.
- [57] J. Self, C.P. Aiken, R. Petibon, J.R. Dahn, *J. Electrochem. Soc.* 162 (2015) A796–A802.
- [58] C.G. Van, de Walle, J. Neugebauer, *Nature* 423 (2003) 626–628.
- [59] H. Meng, J. Zheng, A.J. Lovinger, B.-C. Wang, P.G. Van Patten, Z. Bao, *Chem. Mater.* 15 (2003) 1778–1787.
- [60] M. Cuisinier, C. Hart, M. Balasubramanian, A. Garsuch, L.F. Nazar, *Adv. Energy Mater.* 5 (2015) 1401801.
- [61] E. Endo, K. Tanaka, K. Sekai, *J. Electrochem. Soc.* 147 (2000) 4029–4033.
- [62] M. Grütze, V. Kraft, B. Hoffmann, S. Klamor, J. Diekmann, A. Kwade, M. Winter, S. Nowak, *J. Power Sources* 273 (2015) 83–88.
- [63] Y.-K. Han, S.U. Lee, J.-H. Ok, J.-J. Cho, H.-J. Kim, *Chem. Phys. Lett.* 360 (2002) 359–366.
- [64] J. Qian, W. Xu, P. Bhattacharya, M. Engelhard, W.A. Henderson, Y. Zhang, J.-G. Zhang, *Nano Energy* 15 (2015) 135–144.
- [65] F.A. Soto, Y. Ma, J.M. Martínez, de la Hoz, J.M. Seminario, P.B. Balbuena, *Chem. Mater.* 27 (2015) 7990–8000.
- [66] R.S. Mulliken, *J. Chem. Phys.* 23 (1955) 1833–1840.
- [67] R.S. Mulliken, *J. Chem. Phys.* 23 (1955) 1841–1846.
- [68] E. Endo, M. Ata, K. Tanaka, K. Sekai, *J. Electrochem. Soc.* 145 (1998) 3757–3764.
- [69] D. Bedrov, G.D. Smith, A.C.T. van Duin, *J. Phys. Chem. A* 116 (2012) 2978–2985.
- [70] Y. Wang, S. Nakamura, M. Ue, P.B. Balbuena, *J. Am. Chem. Soc.* 123 (2001) 11708–11718.
- [71] W.Y. Li, H.B. Yao, K. Yan, G.Y. Zheng, Z. Liang, Y.M. Chiang, Y. Cui, *Nat. Commun.* 6 (2015) 7436.
- [72] C.-Z. Zhao, X.-B. Cheng, R. Zhang, H.-J. Peng, J.-Q. Huang, R. Ran, Z.-H. Huang, F. Wei, Q. Zhang, *Energy Storage Mater.* 3 (2016) 77–84.
- [73] C.X. Zu, A. Manthiram, *J. Phys. Chem. Lett.* 5 (2014) 2522–2527.
- [74] X.B. Cheng, H.J. Peng, J.Q. Huang, F. Wei, Q. Zhang, *Small* 10 (2014) 4257–4263.
- [75] C.P. Yang, Y.X. Yin, S.F. Zhang, N.W. Li, Y.G. Guo, *Nat. Commun.* 6 (2015) 8058.
- [76] L.L. Lu, J. Ge, J.N. Yang, S.M. Chen, H.B. Yao, F. Zhou, S.H. Yu, *Nano Lett.* 16 (2016) 4431–4437.
- [77] R. Zhang, X.B. Cheng, C.Z. Zhao, H.J. Peng, J.L. Shi, J.Q. Huang, J.F. Wang, F. Wei, Q. Zhang, *Adv. Mater.* 28 (2016) 2155–2162.
- [78] Y.Y. Lu, Z.Y. Tu, L.A. Archer, *Nat. Mater.* 13 (2014) 961–969.
- [79] X.L. Ji, D.Y. Liu, D.G. Prendiville, Y.C. Zhang, X.N. Liu, G.D. Stucky, *Nano Today* 7 (2012) 10–20.
- [80] D.C. Lin, Y.Y. Liu, Z. Liang, H.W. Lee, J. Sun, H.T. Wang, K. Yan, J. Xie, Y. Cui, *Nat. Nanotechnol.* 11 (2016) 626–632.
- [81] D. Zheng, X.-Q. Yang, D. Qu, *ChemSusChem* 9 (2016) 2348–2350.
- [82] C. Yan, X.-B. Cheng, C.-Z. Zhao, J.-Q. Huang, S.-T. Yang, Q. Zhang, *J. Power Sources* 327 (2016) 212–220.
- [83] N.W. Li, Y.X. Yin, C.P. Yang, Y.G. Guo, *Adv. Mater.* 28 (2016) 1853–1858.
- [84] G.Y. Zheng, S.W. Lee, Z. Liang, H.W. Lee, K. Yan, H.B. Yao, H.T. Wang, W.Y. Li, S. Chu, Y. Cui, *Nat. Nanotechnol.* 9 (2014) 618–623.
- [85] M.F. Wu, Z.Y. Wen, J. Jin, B.V.R. Chowdari, *ACS Appl. Mater. Interfaces* 8 (2016), 2016, pp. 16386–16395.
- [86] A.C. Kozen, C.F. Lin, A.J. Pearse, M.A. Schroeder, X.G. Han, L.B. Hu, S.B. Lee, G.W. Rubloff, M. Noked, *ACS Nano* 9 (2015) 5884–5892.
- [87] Y.H. Gong, K. Fu, J.Q. Dai, A. Gong, X.G. Han, Y.G. Yao, C.W. Wang, Y.B. Wang, Y.N. Chen, C.Y. Yan, Y.J. Li, E.D. Wachsman, L.B. Hu, *Proc. Natl. Acad. Sci. USA* 113 (2016) 7094–7099.
- [88] X. Qu, A. Jain, N.N. Rajput, L. Cheng, Y. Zhang, S.P. Ong, M. Brafman, E. Maginn, L.A. Curtiss, K.A. Persson, *Comp. Mater. Sci.* 103 (2015) 56–67.
- [89] S.-D. Han, N.N. Rajput, X. Qu, B. Pan, M. He, M.S. Ferrandon, C. Liao, K.A. Persson, A.K. Burrell, *ACS Appl. Mater. Interfaces* 8 (2016) 3021–3031.